

Kinematics of the Milky Way from the Gaia EDR3 red giants and sub-giants.

P. N. Fedorov,¹* V. S. Akhmetov,¹ A. B. Velichko,¹ A. M. Dmytrenko¹
and S. I. Denischenko¹

¹*Institute of astronomy of V. N. Karazin Kharkiv national university, Svobody sq. 4, 61022, Kharkiv, Ukraine*

Accepted XXX. Received YYY; in original form ZZZ

ABSTRACT

We present the results of the kinematic investigations carried out with the use of spatial velocities of red giants and sub-giants containing in the *Gaia* EDR3 catalogue. The twelve kinematic parameters of the Ogorodnikov–Milne model have been derived for stellar systems with radii 0.5 and 1.0 kpc, located along the direction the Galactic center – the Sun – the Galactic anticenter within the range of Galactocentric distances R 0–8–16 kpc. By combining some of the local parameters the information related to the Galaxy as a whole has been received in the distance range 4–12 kpc, in particular the Galactic rotational curve, its slope, velocity gradients. We show that when using this approach, there is an alternative possibility to infer the behaviour of the Galactic rotational curve and its slope without using the Galactocentric distance R_{\odot} . The kinematic parameters derived within the Solar vicinity of 1 kpc radius are in good agreement with those given in literature.

Key words: stars: kinematics and dynamics–Galaxy: kinematics and dynamics–solar neighborhood–methods: data analysis–proper motions

1 INTRODUCTION

Investigation of stellar kinematics is an important instrument for the Galactic study. It is based on the analysis of stellar proper motions and radial velocities within various physical and mathematical models. The Ogorodnikov–Milne (O–M, Ogorodnikov (1932); Milne (1935); Ogorodnikov (1965)) model is most commonly used for the stellar kinematics analysis. The model provides the ability to investigate the velocity field in a deformable stellar system. The analysis of the stellar velocity field is usually confined to solving the basic kinematic equations to compute the O–M model parameters in the local coordinate system, which moves together with the Sun about the Galactic centre.

In the last time, some new models are often used to analyse the stellar kinematics. Since stellar proper motions and radial velocities are the components of the velocity vector field, it would be reasonable to use the methods of decomposition of the corresponding stellar velocity field on a set of the vector spherical harmonics (VSH). The approach allows to detect all the systematic constituents present in the stellar velocity field under study, as well as make the mathematically complete kinematic model. Comparison of the decomposition coefficients with model parameters shows whether the models are complete as well as allows to reveal all significant systematics which is not included into the models.

This approach is effective, as demonstrated in a number of papers, for instance Vityazev & Shuksto (2004); Vityazev & Tsvetkov (2005); Makarov & Murphy (2007); Mignard & Klioner (2012); Velichko et al. (2020).

2 THE O–M MODEL EQUATIONS AND FORMING THE LOCAL COORDINATE SYSTEMS

To write mathematically the basic kinematic equations of various models, the Cartesian coordinate system x, y, z is usually applied. The origin of the system coincides with the Solar system barycenter. The x axis points to the Galactic center, y axis coincides with the direction of the Galactic rotation, while z axis is perpendicular to the Galactic plane and complements the right-handed Cartesian coordinate system (see Fig. 1). The given system is called the local rectangular Galactic coordinate system.

In this paper, we use the O–M model which describes the systematic differential stellar velocity field within the vicinity of a chosen point. According to the Helmholtz theorem, the stellar motion may be represented by the sum of velocities, namely the translational motion of the centroid of the corresponding stellar system, as well as its rigid-body rotation and deformation velocities. By the term "centroid" we mean a point that coincides with that moving at a velocity equal to the mean velocity of stars belonging to the given stellar system. This approach has been used, for instance,

* E-mail: pnfedorov@gmail.com (PNF)

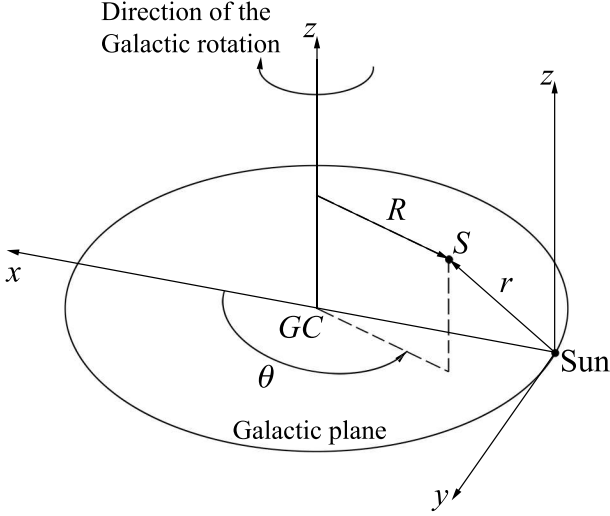


Figure 1. The local rectangular Galactic x, y, z and cylindrical Galactocentric R, θ, z coordinate systems. S is an arbitrary star with the heliocentric distance r .

in the papers by Clube (1972); du Mont (1977); Miyamoto & Soma (1993); Miyamoto & Zhu (1998); Bobylev & Khovrichiev (2011).

In general, representation of the velocity field of a deformable stellar system is based on the general form of expanding the continuous vector function $\mathbf{V}(\mathbf{r})$ which is defined in the vicinity of any point $\mathbf{r}_0(x_0, y_0, z_0)$. In the Cartesian Galactic coordinate system x, y, z the general form of the stellar velocity field expansion $\mathbf{V}(\mathbf{r})$ is as follows:

$$\mathbf{V}(\mathbf{r}) = \mathbf{V}(\mathbf{r}_0 + d\mathbf{r}) = \mathbf{V}(\mathbf{r}_0) + \left(\frac{\partial v_i}{\partial x_k} \right)_0 dx_k + \frac{1}{2!} \left(\frac{\partial^2 v_i}{\partial x_k \partial x_m} \right)_0 dx_k dx_m + \dots \quad (1)$$

where the indexes $k, m = 1, 2, 3$, and the partial derivatives are evaluated at the point $\mathbf{r}_0(x_0, y_0, z_0)$.

When analysing the solar vicinity, we restrict the expansion 1 to the first-order terms and derive the components v_i of the linear velocity field \mathbf{V} at the point located at the heliocentric distance from the Sun $\mathbf{r} = \mathbf{r}_0 + d\mathbf{r}$ as follows:

$$v_i(\mathbf{r}_0 + d\mathbf{r}) = v_i(\mathbf{r}_0) + \frac{1}{2} \left(\frac{\partial v_i}{\partial x_k} - \frac{\partial v_k}{\partial x_i} \right)_0 dx_k + \frac{1}{2} \left(\frac{\partial v_i}{\partial x_k} + \frac{\partial v_k}{\partial x_i} \right)_0 dx_k = v_i(\mathbf{r}_0) + M^- dx_k + M^+ dx_k \quad (2)$$

where $i, k = 1, 2, 3$.

In this equation, $v_i(\mathbf{r}_0)$ is usually interpreted as the mean velocity of the stellar system relative to the Sun, or on the contrary, as the Solar velocity relative to the chosen centroid with the opposite signs, where the components are $v_i(\mathbf{r}_0) = -X_\odot \mathbf{e}_x - Y_\odot \mathbf{e}_y - Z_\odot \mathbf{e}_z$. Thus, finally one can write:

$$v_i(r_0 + dr) = -X_\odot \mathbf{e}_x - Y_\odot \mathbf{e}_y - Z_\odot \mathbf{e}_z + M^- dx_k + M^+ dx_k \quad (3)$$

The matrix elements M^- and M^+ are the partial derivatives of the projections (v_1, v_2, v_3) of the velocity vector on the axes of the rectangular Galactic coordinate system, and they are usually called kinematic parameters.

Components of the antisymmetric matrix

$$M^- = \frac{1}{2} \left(\frac{\partial v_i}{\partial x_k} - \frac{\partial v_k}{\partial x_i} \right)_0 = \omega_{ik} = -\omega_{ki} \quad (4)$$

constitute antisymmetric tensor which is referred to as the tensor of local rotation velocities. It describes the rigid-body rotation of the stellar system under examination about the axis which passes through the stellar centroid with the instant angular velocity ω , and $\omega_1, \omega_2, \omega_3$ are projections of ω on the Galactic axes x, y, z respectively.

The matrix

$$M^+ = \frac{1}{2} \left(\frac{\partial v_i}{\partial x_k} + \frac{\partial v_k}{\partial x_i} \right)_0 = u_{ik} \quad (5)$$

is symmetric, and its components $v_{ik} = v_{ki}$ form the symmetric second-rank tensor which is referred to as the tensor of local deformation velocities. It defines the velocity of deformation motion in the stellar system under study. Usually, it is these components of the tensor that correspond to the forces inducing deformations in the dynamical investigations (Tarapov (2002); Sedov (1970)).

The diagonal components of the symmetric matrix M_{11}^+, M_{22}^+ and M_{33}^+ characterize velocities of relative contractions/expansions of the stellar system along x, y, z axes, while the components $M_{12}^+ = M_{21}^+, M_{23}^+ = M_{32}^+, M_{13}^+ = M_{31}^+$ do velocities of the angular deformations in the (x, y) , (y, z) and (x, z) planes, respectively. Here the velocity of angular deformation means the velocity of changing angles between segments in the planes.

To set a relation between the velocity components $\mathbf{V}(\mathbf{r})$ and the observational data, namely proper motions μ_l and μ_b on the Galactic longitude and latitude, respectively, as well as radial velocity V_r of a star, we project the vector $\mathbf{V}(\mathbf{r})$ on the unit vectors of the spherical Galactic coordinate system $\mathbf{e}_l, \mathbf{e}_b, \mathbf{e}_r$ and introduce the factor $k = 4.74057$ to transform the dimension of stellar proper motions from mas yr^{-1} to $\text{km s}^{-1} \text{ kpc}^{-1}$. Then, the conditional equations for proper motions and radial velocities in the local Galactic coordinate system have the following form:

$$k \mu_l \cos b = X_\odot/r \sin l - Y_\odot/r \cos l - \omega_1 \sin b \cos l - \omega_2 \sin b \sin l + \omega_3 \cos b + M_{12}^+ \cos b \cos 2l - M_{13}^+ \sin b \sin l + M_{23}^+ \sin b \cos l - 0.5 M_{11}^+ \cos b \sin 2l + 0.5 M_{22}^+ \cos b \sin 2l \quad (6)$$

$$k \mu_b = X_\odot/r \cos l \sin b + Y_\odot/r \sin l \sin b - Z_\odot/r \cos b + \omega_1 \sin l - \omega_2 \cos l - 0.5 M_{12}^+ \sin 2b \sin 2l + M_{13}^+ \cos 2b \cos l + M_{23}^+ \cos 2b \sin l - 0.5 M_{11}^+ \sin 2b \cos^2 l - 0.5 M_{22}^+ \sin 2b \sin^2 l + 0.5 M_{33}^+ \sin 2b \quad (7)$$

$$V_r/r = -X_\odot/r \cos l \cos b - Y_\odot/r \sin l \cos b - Z_\odot/r \sin b + M_{13}^+ \sin 2b \cos l + M_{23}^+ \sin 2b \sin l + M_{12}^+ \cos^2 b \sin 2l + M_{11}^+ \cos^2 b \cos^2 l + M_{22}^+ \cos^2 b \sin^2 l + M_{33}^+ \sin^2 b \quad (8)$$

The equations given above define the differential stellar velocity field and contain 12 unknown parameters.

The local Galactic coordinate system can be introduced at any arbitrary point of the Galactic plane provided that one know coordinates x, y, z , spacial velocities V_x, V_y, V_z of the point (for instance, a star) and for all stars located within the corresponding vicinity. Taking the Galactocentric distance of the Sun to be equal to $R_\odot = 8.0$ kpc (Valleé (2017)), one can make the transition from the local

Galactic coordinate system with the origin at the barycenter of the Solar system to one with the origin at the chosen point. The corresponding transformation takes into account, in general, transposing the origin of the Galactic coordinate system and turning the coordinate axes. The x' -axis of the new coordinate system always points to the Galactic center, the y' -axis coincides with the direction of the Galactic rotation, and the z' one is perpendicular to the Galactic plane. The procedure would translocate the fictitious observer from the barycenter of the Solar system to the point given by the origin of the new coordinate system.

Thus, one can write the conditional equations of the O–M model in the chosen coordinate system and estimate the kinematic parameters in the vicinity of each chosen point. It is evident that these kinematic parameters are local, since they characterize the stellar kinematics within a small spacial volume, for instance within a spherical area with a given radius r' . Nevertheless, such an analysis of stellar kinematics in various Galactic parts provides insight into behaviour of some global kinematic parameters, i.e. those related to the entire Galaxy.

In this paper, we present estimations within the O–M model of the kinematic parameters for stellar systems located along the direction the Galactic center – the Sun – the Galactic anticenter. In this case, the origin of the coordinate system is shifting along the X -axis relative to the Sun with the step of 250 pc, without any rotations of the coordinate system.

3 SOLVING THE PROBLEM

For the analysis, we use the *Gaia* EDR3 data (Gaia collaboration et al. (2016b, 2021a)) of ~ 7.21 million stars, for which, in addition to proper motions, radial velocities were also derived within the second release of the *Gaia* mission (Katz et al. (2019)). The diagram color $BP - RP$ – absolute magnitude M_G for 10% of these stars is shown in Fig. 2. The diagram is rough because extinction was not taken into account. Using the straight lines in Fig. 2, the stars were split into the main sequence stars (located below the lines), and higher luminosity stars, such as sub-giants and giants (located above the lines)

The Fig. 3 shows the distribution of number of stars with the heliocentric distance r . r were computed from parallaxes as $1/\pi$. As one can see from the Fig. 3, the distance range corresponding to the main sequence stars occupies the relatively narrow range of the Galactocentric distances $7 \text{ kpc} < R < 9 \text{ kpc}$. On the contrary, sub-giants and red giants cover a much wider Galactocentric distance range, $0 \text{ kpc} < R < 16 \text{ kpc}$. Therefore, the latter stellar sample is better to trace the Galactic kinematics. The total amount of sub-giants and red giants is 4.5 million.

Each point, from which the observations would be made by a fictitious observer, is placed on the x axis. The centers of the spheres, restricting spacial volumes that contain stars around each point, are located every 250 pc from $R = 0 \text{ kpc}$ to 16 kpc . The radii r' of the spheres have been set equal to 500 pc or 1000 pc.

To improve the accuracy of the derived results, in the specific coordinate system the special procedure has been carried out consisting in exclusion stars whose velocities deviate from the average value by more than 3σ . The rejection procedure has been carried out in each pixel on the celestial sphere that would be visible from the specific point. The pixelization has been made according to the HEALPix scheme (The Hierarchical Equal Area iso-Latitude Pixelization, Gorsky et al. (2005)) with $N_{\text{side}} = 10$ that allows to divide

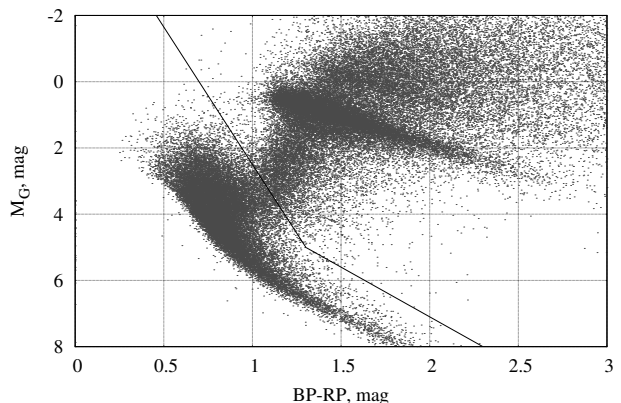


Figure 2. Selection of red giants and sub-giants.

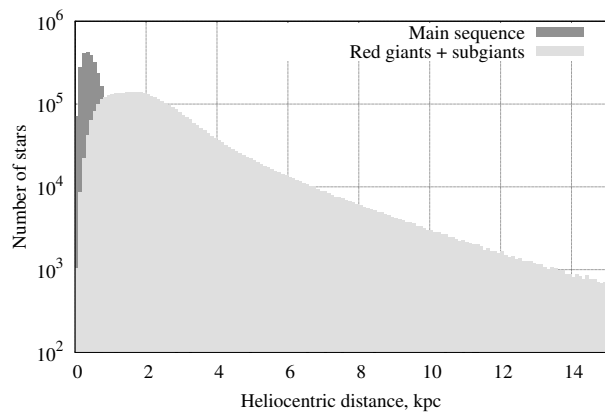


Figure 3. The number of main sequence stars and red giants plus sub-giants depending on the heliocentric distance.

the sphere onto 1200 equal areas (pixels). The pixelization has been applied only for excluding stars.

Once the rejection procedure has been applied, the individual values of stellar positions, parallaxes, proper motions, and radial velocities has been used to solve by the linear least square method (LSM) the O–M model equations written for each local Galactic coordinate system. As a result, the derived kinematic parameters characterize the stellar velocity field within vicinity of each given point.

The O–M model parameters allow to estimate a number of kinematic and physical parameters related to the Galaxy as a whole. Within the simplified form of the O–M model is usually called as the Oort-Lindblad one Ogorodnikov (1965), the stellar velocity field is assumed to be axisymmetric. Herewith, the system rotates in the Galactic plane only, i.e. $\omega_3 = |\omega|$ while ω_1 and ω_2 are equal to zero. In this case the value of $M_{21}^- = \omega_3$ corresponds to the Oort constant B . The deformation also exists in the Galactic plane only, i.e. it is characterized by the Oort constant $A = M_{12}^+$, while M_{13}^+ and M_{23}^+ are equal to zero. Contractions/expansions M_{11}^+ , M_{22}^+ , M_{33}^+ along the corresponding axes are not taken into account. The Oort constants are usually used in papers on kinematics to characterize the Galactic rotation (for instance, Bovy (2017); Vityazev et al. (2018); Chengdong et al. (2019); Tsvetkov (2019)).

Thus, the angular rotation velocity of the Galaxy in the Solar vicinity is equal to

$$\Omega = A - B = M_{12}^+ - \omega_3 \quad (9)$$

In general, if not to restrict the stellar velocity field, taking into account the fact that the pairs (ω_1, M_{23}^+) and (ω_2, M_{13}^+) in the corresponding planes are analogous to the Oort constants B and A respectively, for an arbitrary centroid located at the Galactocentric distance R one can compute the angular rotation of the Galaxy velocity Ω_R :

$$\Omega_R = \sqrt{(M_{12}^+ - \omega_3)^2 + (M_{13}^+ - \omega_2)^2 + (M_{23}^+ - \omega_1)^2} \quad (10)$$

It is obvious that, knowing values of the Solar velocity components X_\odot, Y_\odot and Z_\odot , or velocity of an arbitrary point where the origin of the coordinate system is placed, relative to the centroids, one can compute the velocity module V_\odot and the apex coordinates L_\odot and B_\odot :

$$V_\odot = \sqrt{X_\odot^2 + Y_\odot^2 + Z_\odot^2} \quad (11)$$

$$\text{tg } L_\odot = \frac{Y_\odot}{X_\odot}, \quad \text{tg } B_\odot = \frac{Z_\odot}{\sqrt{X_\odot^2 + Y_\odot^2}} \quad (12)$$

4 KINEMATIC PARAMETERS OF THE O–M MODEL

It is worth noting that, at this stage of our kinematic analysis the O–M model parameters derived out of the range of Galactocentric distances 4–12 kpc, are not assumed to be reliable due to a variety of reasons. This is, first of all, significant decreasing the amount of stars (the number of stars containing in each stellar system is given in tables A1, A2). As a result, the uncertainties of the derived parameters increase. Moreover, the error bars grow since the astrometric parameters become less accurate with the heliocentric distance to the sources. In third place, since the O–M model is linear, it can be confidently applied if the radius of the stellar system under examination r' is much less than the Galactocentric distance to the stellar system R , i.e. $r' \ll R$. Unfortunately, this condition is not fulfilled when analysing the stellar systems which are close to the Galactic center ($R < 4$ kpc), although toward the Galactic anticenter the condition is well fulfilled.

However, the main reason of unreliability is due to our estimations of the parameters of rotation ω_1, ω_2 and deformation in yz and xz planes are actually the values averaged over the northern and southern Galactic hemispheres. In the papers by Vityazev & Tsvetkov (2014); Velichko et al. (2020) the stellar kinematics was analysed using the vector spherical harmonics. The authors have shown that the values of the deformation velocity component M_{12}^+ in the xy plane and rotation velocity ω_3 are equal in the northern and southern Galactic hemispheres. The values of the rotation velocity components ω_1, ω_2 as well as deformation velocity components M_{23}^+ and M_{13}^+ have different signs in the northern and southern hemispheres while their modules are virtually equal. Therefore, it is not surprising that we see in Fig. 4 the near zero averaged values of these parameters within the range $4 < R < 12$ kpc, since the centers of the spheres with radii $r' = 500$ pc and 1000 pc are located in the Galactic plane and encompass the stars of both the northern and southern Galactic hemispheres. However, it would

be wrongly to consider as actual any deviations of the values from zero out of the Galactocentric range 4–12 kpc, since the deviations can be caused, for instance, by shifting the LSM solutions due to the celestial sphere is not covered uniformly (distribution of objects through the whole celestial sphere is not uniform). Nevertheless, we show in figures the Galactocentric distance range from 0 kpc to 16 kpc to have at least some understanding of behaviour of the kinematic parameters near the Galactic center as well as in its outer part.

4.1 Components of the rotational tensor

As one can see from Fig. 4 (left panel), in the range 4–12 kpc the parameters ω_1 and ω_2 are virtually equal to zero, while ω_3 gradually changes from $-30 \text{ km s}^{-1} \text{ kpc}^{-1}$ to $-10 \text{ km s}^{-1} \text{ kpc}^{-1}$ and at the Solar distance has the value $\omega_3 = -13.5 \pm 0.08 \text{ km s}^{-1} \text{ kpc}^{-1}$ which is found to be in good agreement with those given in numerous papers (for instance, Vityazev & Tsvetkov (2012); Bovy (2017); Vityazev et al. (2018); Chengdong et al. (2019); Tsvetkov (2019); Velichko et al. (2020)). The behaviour of the components ω_1, ω_2 and ω_3 indicate that the vectors of instantaneous angular rotational velocity of the corresponding stellar systems are virtually perpendicular to the Galactic plane, and in the modulus almost coincide with the value ω_3 . Out of range 4–12 kpc the components of the rotation vector ω_1 and ω_2 slightly change but we cannot guarantee the behaviour to be realistic, for the reasons mentioned above.

4.2 Components of the deformation velocity tensor

The right panel of Fig. 4 demonstrates the deformation components $M_{12}^+, M_{23}^+, M_{13}^+$ in the corresponding planes. One can clearly see that in the range 4–8 kpc M_{12}^+ gradually increases from 0 to about $16 \text{ km s}^{-1} \text{ kpc}^{-1}$ that followed by a decrease up to 0 at $R = 12$ kpc. The value of $M_{12}^+ = 14.92 \pm 0.08 \text{ km s}^{-1} \text{ kpc}^{-1}$ at the Solar distance also is in good agreement with estimations derived in numerous papers (the same ones as in subsection 4.1). As in the case of rotational components, in the range 4–8 kpc the deformation tensor components M_{13}^+ and M_{23}^+ are virtually equal to zero, while within the entire distance range 0–16 kpc their behaviour is very similar to that for ω_2 and ω_1 but with opposite sign.

4.3 Diagonal components of the deformation velocity tensor

Left panel of Fig. 5 shows dependencies on Galactocentric distance of the kinematic parameters M_{11}^+, M_{22}^+ and M_{33}^+ which characterize contractions/expansions of the stellar systems under study along $x, y,$ and z axes, respectively. As one can see in left panel of Fig. 5, the behaviour of M_{11}^+ shows pronounced peculiarity in the Solar vicinity. At the same time, in range 4–12 kpc M_{22}^+ and M_{33}^+ do not show such drastic changes in their behavior but demonstrate near zero variations. This indicates relatively small contractions/expansions along the y and z axes within the specified distance range. The x -axis direction to the Galactic center (vertex), given inaccurate, may be one of the reasons of the peculiar behaviour of the parameter M_{11}^+ . However, to unambiguously establish the real reasons of the behaviour requires additional investigations which will be present in our future papers.

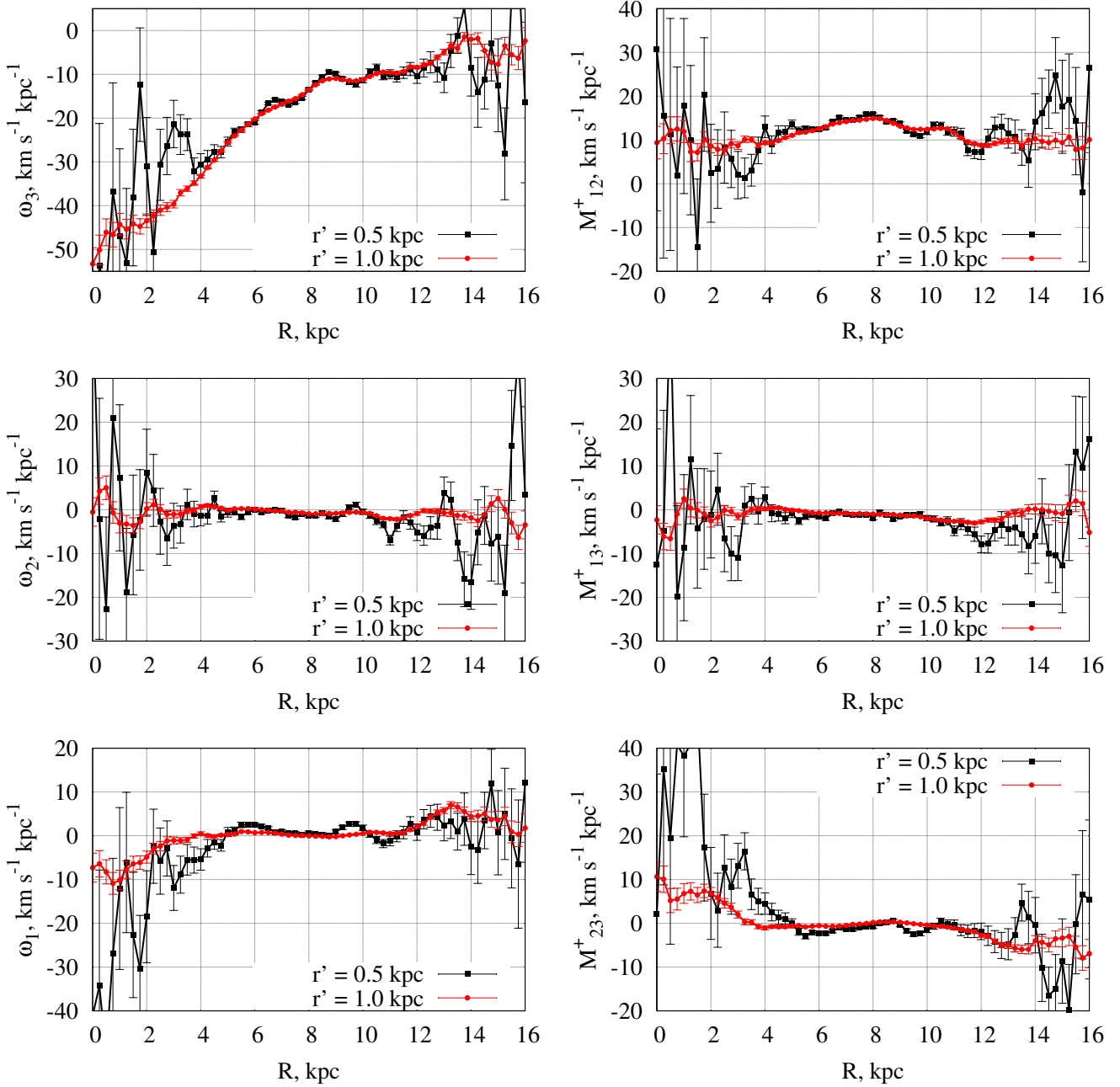


Figure 4. The components of local rotation velocities tensor ω_3 (Oort B), ω_2 , ω_1 (left panel), and the components of deformation velocity tensor M_{12}^+ (Oort A), M_{13}^+ , M_{23}^+ (right panel) as a function of the Galactocentric distance.

4.4 Components of the Solar velocity relative to different centroids and coordinates of the Solar apex

Right panel of Fig. 5 shows the components of the linear Solar velocity, while its modulus and coordinates of the Solar apex are given in Fig. 6 as functions of the Galactocentric distance.

As one can see from the right panel of Fig. 5, the component of the Solar velocity vector X_\odot relative to centroids located within the range from 7 to 10 kpc undergoes noticeable changes, and at $R = 8$ kpc has minimal value equal to $8.34 \pm 0.06 \text{ km s}^{-1} \text{ kpc}^{-1}$ at $R = 8.75$ kpc. It worth noting that within the specified distance range the parameter M_{11}^+ also changes significantly. It is obvious that the changes also affect the values of the Solar apex coordinates

L and B . In this distance range, one can see that there are less noticeable but still obvious variations of the parameters M_{12}^+ and ω_3 . The values of X_\odot , Y_\odot and Z_\odot relative to the centroid located at the Solar distance, as well as the Solar apex coordinates are in good agreement with those given in other papers (for instance, Vityazev & Tsvetkov (2014); Velichko et al. (2020)), that indicates the behaviour of these Solar velocity components is realistic.

Thus, we have a very interesting result. We know that the Solar velocity relative to the centroids taken with opposite sign is equal to the velocity of centroids relative to the Sun. On the other hand, the Solar velocity modulus relative to the Galactic center is constant. Hence, the behaviour of the centroids' linear velocity components

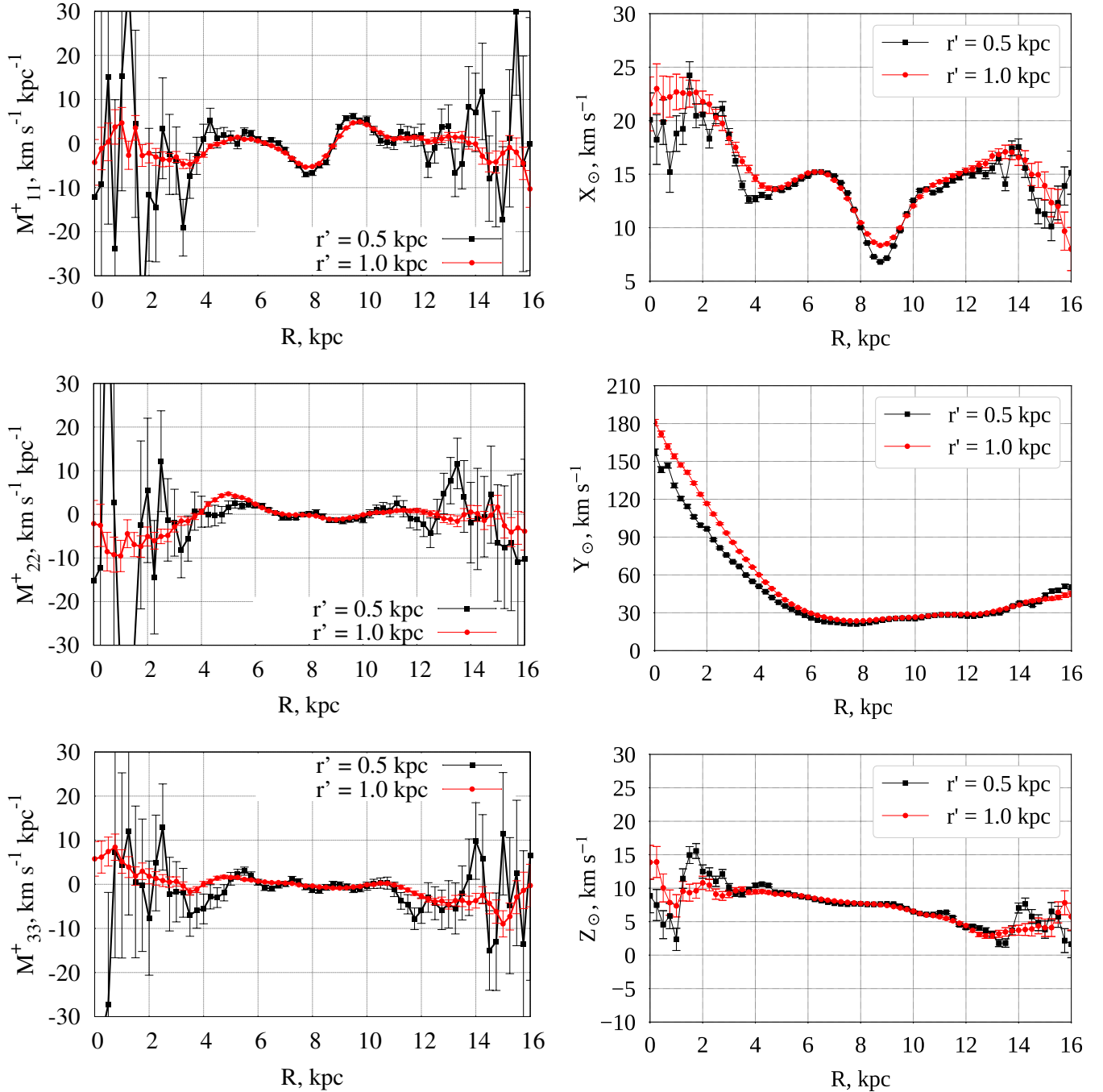


Figure 5. The diagonal components of deformation velocity tensor (left panel) and the Solar motion components (right panel) as a function of the Galactocentric distance.

relative to the Galactic center taken with opposite sign has to follow that of the X_{\odot} , Y_{\odot} and Z_{\odot} components. Since the absolute values of the Solar velocity components relative to the Galactic center are not known, it is impossible to establish the offsets on axes for the functions X_{\odot} , Y_{\odot} and Z_{\odot} , but their behaviour is determined reliably. In particular, the behaviour of the function $Y_{\odot}(R)$ have to reproduce that of the Galactic rotational curve $V_{\text{rot}}(R)$. Moreover, since the values of the Solar peculiar velocity component Y_{\odot} have been derived only from the *Gaia* data, not using Galactocentric distances, we derive the behaviour of the Galactic rotational curve

more accurately compared to the traditional estimation present in subsection 5.1.

Irregular behaviour of the component X_{\odot} may be explained by influence of the Gould Belt's stellar velocity field. The stellar kinematics of this local system with the characteristic radius of about 0.5 kpc is known to differ from that of stars do not belonging to it (see, for instance, [Bobylov \(2004, 2014\)](#); [Alves and all. \(2020\)](#)).

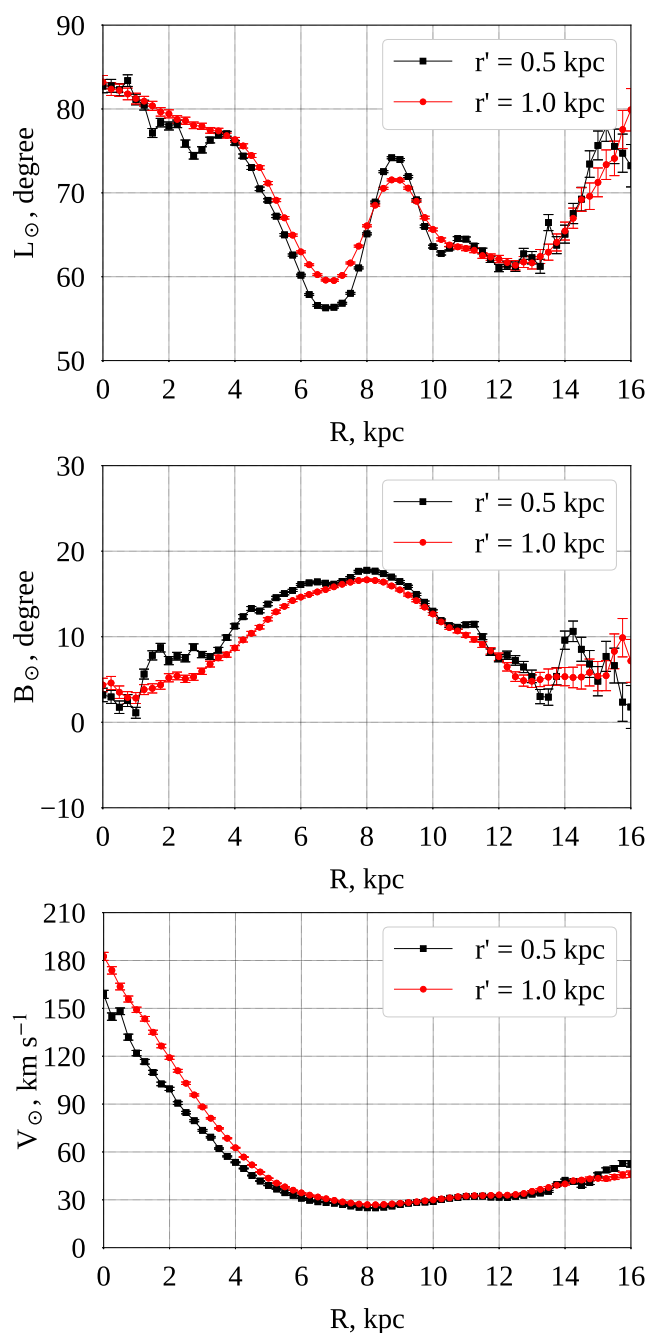


Figure 6. Coordinates of the Solar apex and the Solar velocity modulus as a function of the Galactocentric distance.

4.5 Components of the angular Galactic rotational velocity

Fig. 10 shows the components of the angular Galactic rotational velocity vector Ω derived from the analysis of the stellar systems under examination. Fig. 7 shows the vector's modulus as a function of the Galactocentric distance R . One can clearly see from the figures that in the range 4–12 kpc the components of the angular Galactic rotational velocity are nearly zero, and therefore the Galactic rotation vector within the range are virtually perpendicular to the Galactic plane. The value of Ω at the Solar distance is about $30 \text{ km s}^{-1} \text{ kpc}^{-1}$.

Finally, We emphasize that the kinematic parameters derived in this work for the Solar centroid are very close to those published

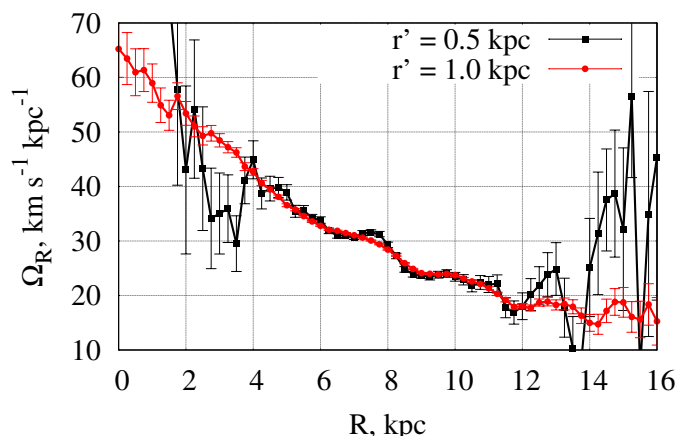


Figure 7. The modulus of the angular Galactic rotational velocity $|\Omega|$ as a function of the Galactocentric distance.

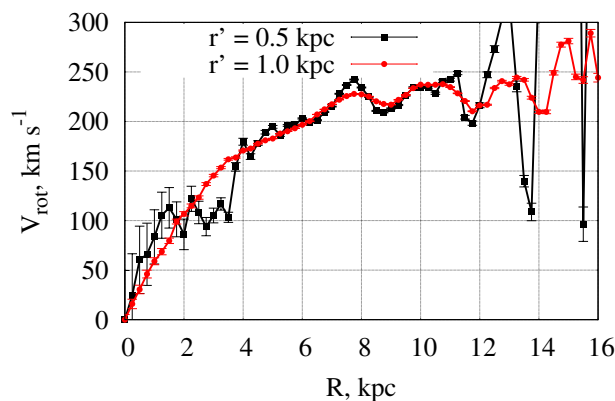


Figure 8. Circular velocity of Galaxy as a function of the Galactocentric distance (Galactic rotation curves).

in earlier works mentioned above. This indicates that all the values derived for other centroids located along the x -axis are adequate.

5 INTERPRETATION OF THE KINEMATIC PARAMETERS GIVEN IN THE CYLINDRICAL COORDINATE SYSTEM

To interpret the derived results and get some information about the Galaxy as a whole we move to the Galactocentric coordinate system (Miyamoto & Soma (1993); Bobylev (2006); Vityazev & Tsvetkov (2012), Fig.1). As before, here we have in mind that the components of the rotational and deformation velocity tensors defined in the vertical planes xz and yz have opposite signs in the northern and southern Galactic hemispheres. When solving the equations by the LSM this regularity may be broken due to stellar distribution over the sphere is not uniform, especially in spatial areas which are distant from the Sun. This may result in biases in the least squares solutions.

The elements of the rotational and deformation tensors in the local Galactic coordinate system are related to the stellar velocity field components V_R , V_θ and V_z in the cylindrical Galactocentric coordinate system (R, θ, z) in the following way:

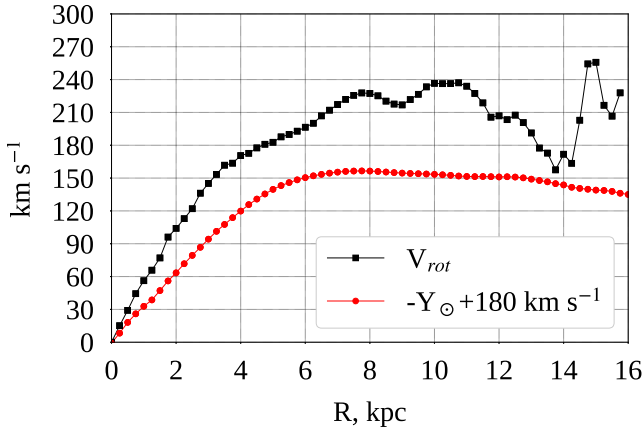


Figure 9. Comparison of the behaviours of the Galactic rotational curves derived from the equation 15 and using the component Y_{\odot} .

$$M = 0.5 \begin{pmatrix} 2M_{11}^+ & M_{12}^+ + M_{12}^- & M_{13}^+ + M_{13}^- \\ M_{21}^+ + M_{21}^- & 2M_{22}^+ & M_{23}^+ + M_{23}^- \\ M_{31}^+ + M_{31}^- & M_{32}^+ + M_{32}^- & 2M_{33}^+ \end{pmatrix} = \begin{pmatrix} \frac{\partial V_R}{\partial R} & \frac{1}{R} \frac{\partial V_R}{\partial \theta} - \frac{V_{\theta}}{R} & \frac{\partial V_R}{\partial z} \\ \frac{\partial V_{\theta}}{\partial R} & \frac{1}{R} \frac{\partial V_{\theta}}{\partial \theta} + \frac{V_R}{R} & \frac{\partial V_{\theta}}{\partial z} \\ \frac{\partial V_z}{\partial R} & \frac{1}{R} \frac{\partial V_z}{\partial \theta} & \frac{\partial V_z}{\partial z} \end{pmatrix} \quad (13)$$

5.1 Galactic rotational velocity in the centroids' vicinity

The components of the Galactocentric velocities V_R , V_{θ} and V_z as well as their derivatives can be expressed via the combinations of the O–M model parameters. Thus,

$$\frac{V_{\theta}}{R} + \frac{1}{R} \frac{\partial V_R}{\partial \theta} = (\omega_3 - M_{12}^+). \quad (14)$$

Since the stellar system's angular rotational velocity components in the xz and yz planes (Fig. 4) are nearly zero within the distance range 4–12 kpc, the radical expression 10 contains only the first term. As a result, the stellar velocity field within the specified distance range may be considered as axisymmetric. Therefore, we assume that

$$\frac{\partial V_R}{\partial \theta} = 0.$$

Then, given the Galactic rotation is opposite to the direction of reference of the azimuth angle θ , we can compute the circular velocity of the local coordinate system V_{rot} (i.e. Galactic rotational velocity) as follows:

$$V_{\text{rot}} = -V_{\theta} = (M_{12}^+ - \omega_3)R = \Omega_R R \quad (15)$$

Fig. 8 shows the linear circular Galactic rotational velocity $V_{\text{rot}} = \Omega_R R$ as a function of the Galactocentric distance R . As one can see from the figure, the values of V_{rot} determined in the Solar vicinity is in good agreement with those given in numerous papers (see above), and it is equal to about $227.36 \pm 0.11 \text{ km s}^{-1}$. The dependency, commonly referred to as the Galactic rotational curve,

is reliable only within the distance range 4–12 kpc. Unfortunately, out of the specified range the values of V_{rot} should not be trusted. Nevertheless, as mentioned above, Fig. 8 demonstrates the entire distance range from 0 to 16 kpc to get insight into values and behaviour of V_{rot} near the Galactic center and at its outer part.

For comparison, Fig. 9 also shows the dependency of Y_{\odot} on R , derived only from the peculiar Solar velocity relative to the centroids given with opposite sign. These two curves have been align by ordinate at $R = 0 \text{ kpc}$.

5.2 Radial gradient of the Galactic rotational velocity

The radial gradient of the Galactic rotational velocity, or the slope of the Galactic rotational curve, is defined by the relation:

$$\frac{\partial V_{\text{rot}}}{\partial R} = -(M_{12}^+ + \omega_3) \quad (16)$$

The top panel of Fig. 10 shows $\partial V_{\text{rot}}/\partial R$ as a function of R . It is clearly seen that the values and behaviour of the slope within the distance range from 0 to about 8 kpc are noticeably different from those in the range 8–16 kpc. In the latter case, the curve's slope decreases, and its magnitude oscillates around $\partial V_{\text{rot}}/\partial R = -2 - 5 \text{ km s}^{-1} \text{ kpc}^{-1}$, that, in principle, does not contradict to the behaviour of the Galactic rotational curve.

At the same time, we can derive the slope of the Galactic rotational curve via differentiation of Y_{\odot} by R . For comparison, Fig. 11 demonstrates the numerical derivative of the function Y_{\odot} by R which is the slope of the Galactic rotational velocity derived only from the analysis of the peculiar Solar velocity relative to the centroids. Its values are in good agreement with those computed from the relation 16.

5.3 Vertical gradient of the Galactic rotational curve

The vertical gradient of the Galactic rotational velocity $\partial V_{\text{rot}}/\partial z$ is defined as follows:

$$\frac{\partial V_{\text{rot}}}{\partial z} = M_{23}^+ - \omega_1 \quad (17)$$

The analysis of the kinematic parameter using vector spherical harmonics was carefully carried out in the papers by Vityazev & Tsvetkov (2014); Velichko et al. (2020). It was shown that the gradients derived from the *Gaia* DR2 data in the northern and southern hemispheres have opposite signs and their modules are nearly equal. Therefore, when calculating over the entire sphere, within the distance range 4–12 kpc $\partial V_{\text{rot}}/\partial z$ is nearly zero but still non-zero. The fact is given in the left panel of Fig. 10 (in the middle) that shows the dependency of $\partial V_{\text{rot}}/\partial z$ on R .

5.4 Galactic warp

The relation

$$\Sigma = -\frac{1}{R} \frac{\partial V_z}{\partial \theta} = \omega_1 + M_{23}^+ \quad (18)$$

is usually interpreted as kinematic manifestation of the local Galactic warp. Its values were derived for the Solar vicinity by Miyamoto & Soma (1993); Zhu (2000); Mignard (2000); Vityazev & Tsvetkov (2012). In the present paper the value is found to be nearly zero within the entire distance range (the right panel of Fig. 10, in the middle).

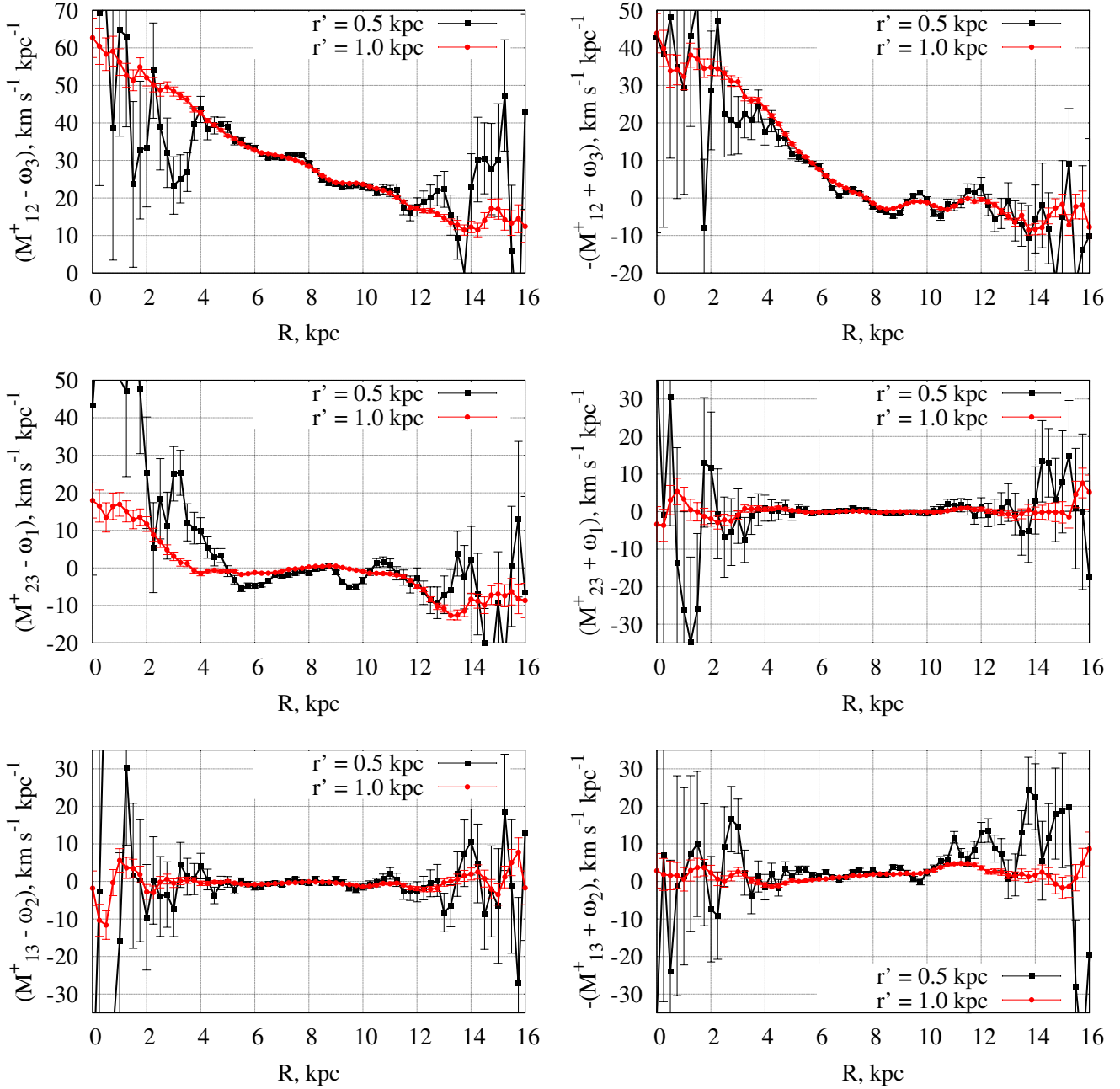


Figure 10. The component of the angular Galactic rotational velocity vector Ω and gradients of components Galactocentric velocity as a function of the Galactocentric distance.

5.5 Gradient of the vertical velocity component along the radius-vector

The gradient of the vertical component of the stellar velocity field along the radius-vector is defined as:

$$\frac{\partial V_z}{\partial R} = \omega_2 - M_{13}^+ \quad (19)$$

It is shown in the left panel of Fig. 10 (bottom row). One can see that its values are nearly zero within the distance range 2–14 kpc.

5.6 Vertical gradient of the Galactic expansion velocity

The vertical gradient of the Galactic expansion velocity can be found from the equation:

$$\frac{\partial V_R}{\partial z} = -(\omega_2 + M_{13}^+) \quad (20)$$

Its behaviour is given in the right panel of Fig. 10 (bottom row). One can see that its numerical values are small but statistically significant. Besides, its values grow slowly with distance up to about 11.5 kpc. It is obvious that more accurate estimations of the given gradients may be established only solving similar tasks for the northern and southern hemispheres separately.

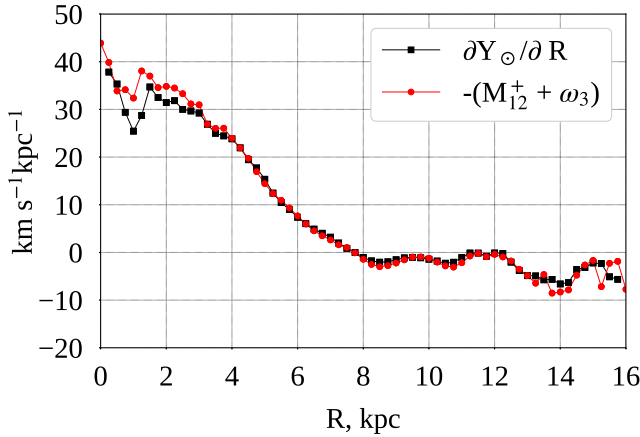


Figure 11. Comparison of the slope of the Galactic rotational curve $-(M_{12}^+ + \omega_3)$ and the numerical derivative $\partial Y_{\odot}/\partial R$.

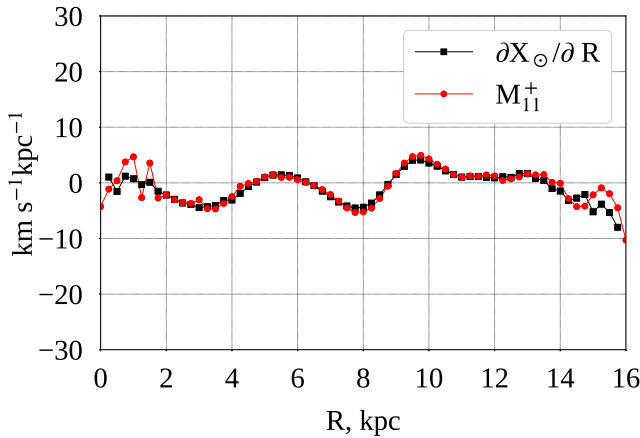


Figure 12. Comparison of the component of deformation velocity M_{11}^+ along axis x and the numerical derivative $\partial X_{\odot}/\partial R$.

5.7 Relationships between the diagonal components of the deformation tensor and the stellar velocity field components V_R , V_{θ} and V_z

$$\frac{\partial V_R}{\partial R} = M_{11}^+ \quad (21)$$

$$\frac{V_R}{R} + \frac{1}{R} \frac{\partial V_{\theta}}{\partial \theta} = M_{22}^+ \quad (22)$$

$$\frac{\partial V_z}{\partial z} = M_{33}^+ \quad (23)$$

As mentioned above, the behaviour of the Solar velocity components X_{\odot} , Y_{\odot} and Z_{\odot} reflects that of centroids' linear velocity components relative the Galactic center. This obviously implies that the centroid's velocity vector has not only the Y_{\odot} component related to V_{θ} but X_{\odot} and Z_{\odot} components related to V_R and V_z , respectively. The parameters X_{\odot} and M_{11}^+ shown in the top panel of Fig. 5 have been computed as independent unknowns by solving the O–M model equations. Therefore, the excellent agreement between the M_{11}^+ dependency and that derived by numerical differentiation of the function X_{\odot} by R is an evidence of both actuality and reliability of their estimations (see Fig. 12).

6 SUMMARY AND CONCLUSIONS

The method applied in the present paper for deriving the O–M model kinematic parameters with the use of stellar spatial velocities, allowed both to estimate the parameters in a specific local Galactic region and to compute a number of global characteristics related to much larger Galactic volumes. Besides, this approach have demonstrated appearance of new, alternative possibilities, in particular, to trace the behaviour of the Galactic rotational curve and its slope. The present results demonstrate the ability of the method to check consistency and reliability of the derived parameters. Numerical estimations of the kinematic parameters as well as their errors are given in Tables A1, A2 of the Appendix A.

Since there are some processes in the Galaxy which have opposite directions in the northern and southern hemispheres, when analysing the stellar velocity field over the entire sphere, they compensate each other and become undetectable. Therefore, the final interpretation of the derived results requires additional investigations of the stellar velocity field in the northern and southern Galactic hemispheres separately. In the near future, we plan to publish the results of further research aimed at eliminating the uncertainties appeared at large and small Galactocentric distances as well as enlarging the volume of the Galactic spatial area under study.

7 ACKNOWLEDGEMENTS

This work has made use of data from the European Space Agency (ESA) mission *Gaia* (<https://www.cosmos.esa.int/gaia>), processed by the *Gaia* Data Processing and Analysis Consortium (DPAC, <https://www.cosmos.esa.int/web/gaia/dpac/consortium>). Funding for the DPAC has been provided by national institutions, in particular the institutions participating in the *Gaia* Multilateral Agreement.

DATA AVAILABILITY

The used catalogue data is available in a standardised format for readers via the CDS (<https://cds.u-strasbg.fr>). The software code used in this paper can be made available upon request by emailing the corresponding author.

References

- Alves J., Zucker C., Goodman A.A., Speagle J., Meingast S., Robitaille T., Finkbeiner D., Schlafly T., Grnee G. 2020, *Nature*, 578, 237–239
- Bobylev V. V. 2004, *Astron. Let.*, 30, No. 11, 785–796
- Bobylev V. V. 2006, *Astron. Let.*, 32, No. 9, 676–690
- Bobylev V. V., Khovritchev, M. Yu. 2011, *MNRAS*, 417, 1952–1963
- Bobylev V. V. 2014, *Astrophysics*, 57, 4
- Bovy J. 2017, *MNRAS*, 468, L63
- Clube S. V. M. 1972, *MNRAS*, 159, 289–314
- Chengdong L., Gang Zh., Chengqun Y. 2019, *ApJ*, 872:205
- Gaia collaboration et al. 2016, *A&A*, 595, A2
- Gaia collaboration et al. 2021, *A&A*, 649, A1
- Gorski K. M., Hivon E., Banday A. J., Wandelt B. D., Hansen F. K., Reinecke M., Bartelmann M. 2005, *AJ*, 622, pp. 759–771
- Katz D., Sartoretti P., Cropper M., et al. 2019, *A&A*, 622, A205
- Makarov V. V. & Murphy D. W. 2007, *AJ* 134, 367–375
- Mignard F. 2000, *A&A*, 354, 522–536
- Mignard F. & Klioner, S. 2012, *A&A*, 547, A59
- Milne E. A. 1935, *MNRAS*, 95, 560.
- Miyamoto M. & Zhu Z. 1998, *AJ*, 115, 1483.

- Miyamoto M. & Soma M. 1993, *AJ*, 105, 691-701.
- du Mont B., 1977, *A&A*, 61, 127–132
- Ogorodnikov K. F. 1965, *Dynamics of stellar systems*, Fizmatgiz, Moscow
[in russian]
- Ogorodnikov K. F. 1932, *Z. Astrophys.*, 4, 190
- Sedov L. I. 1970, *Continuum mechanics*, V. 1., Science, Moscow, 492 pp.
[in russian]
- Tsvetkov A., Amosov F. 2019, *Astron. Lett.*, 45, No. 7, 517-528
- Tarapov I. E. 2002, *Continuum mechanics. V. 2: General laws of kinematics and dynamics*. 2002, Gould pages, Kharkov, 516 pp. [in russian]
- Valleé J. P. 2017, *Astrophys Space Sci*, 362, 7971
- Vityazev, V. V., Popov, A. V., Tsvetkov, A. S., Petrov, S. D., Trofimov, D. A., Kiyayev, V. I. 2018, *Astron. Lett.*, 44, 4, pp. 236-247
- Vityazev V. V., Tsvetkov A. S. 2014, *MNRAS*, 442, 1249–1264
- Velichko A. B., Fedorov P. N., Akhmetov V. S. 2020, *MNRAS*, 494, pp. 1430-1447
- Vityazev V. V., Tsvetkov A. S. 2012, *Astron. Lett.*, 38, 7, pp. 411-427
- Vityazev V. V., Tsvetkov A. S. 2005, *Vestn. Spb. Univ., Ser.1*, 1
- Vityazev V. V., Shuksto A. K. 2004, in *ASP Conference Series*, Vol. 316, *Order and Chaos on Stellar and Planetary Systems*, ed. G. Byrd, K. Kholshcheynikov, A. Mylläri, I. Nikiforov & V. Orlov, 230
- Zhu Z. 2000, *Publ. Astron. Soc. Japan*, 52, 1133.

APPENDIX A: KINEMATIC PARAMETERS OF THE O–M MODEL

This paper has been typeset from a $\text{\TeX}/\text{\LaTeX}$ file prepared by the author.

Table A1. The O–M model parameters for stellar systems with $r' = 1.0$ kpc. R is the Galactocentric distance to centroids, in kpc; N_{stars} is the number of stars containing in each stellar system; the Solar motion components are in km s^{-1} ; the other O–M model parameters are in $\text{km s}^{-1} \text{ kpc}^{-1}$.

R	N_{stars}	X_{\odot}	Y_{\odot}	Z_{\odot}	ω_1	ω_2	ω_3
16.00	202	8.01±2.02	44.98±2.02	5.75±2.02	1.76±3.24	-3.47±3.19	-2.36±3.00
15.75	242	9.68±1.78	43.85±1.78	7.83±1.78	0.32±2.79	-6.32±2.77	-6.30±2.63
15.50	296	12.00±1.57	42.16±1.57	6.39±1.57	0.89±2.50	-3.02±2.47	-5.53±2.32
15.25	372	12.35±1.33	41.30±1.33	4.11±1.33	4.43±2.09	0.10±2.04	-3.51±1.96
15.00	469	13.92±1.30	41.00±1.30	4.09±1.30	3.58±2.01	2.59±2.01	-7.68±1.91
14.75	619	14.95±1.18	40.19±1.18	4.37±1.18	3.71±1.78	1.37±1.82	-7.30±1.72
14.50	809	14.97±1.04	39.41±1.04	3.90±1.04	5.00±1.58	-1.09±1.59	-4.61±1.49
14.25	1055	16.32±0.88	38.40±0.88	3.82±0.88	4.53±1.33	-2.51±1.34	-1.81±1.29
14.00	1383	16.56±0.74	36.25±0.74	3.72±0.74	4.38±1.13	-1.84±1.13	-1.99±1.07
13.75	1815	17.05±0.69	35.10±0.69	3.64±0.69	5.53±1.04	-1.37±1.04	-1.46±0.98
13.50	2396	17.08±0.63	33.42±0.63	3.47±0.63	6.57±0.94	-1.31±0.94	-4.09±0.88
13.25	3160	16.84±0.53	32.23±0.53	3.18±0.53	6.99±0.80	-0.73±0.80	-3.47±0.75
13.00	4183	16.70±0.45	30.97±0.45	2.96±0.45	5.76±0.69	-0.71±0.69	-4.92±0.64
12.75	5438	16.00±0.39	29.79±0.39	2.88±0.39	5.30±0.59	-0.33±0.59	-6.11±0.55
12.50	7209	15.87±0.32	29.07±0.32	3.09±0.32	4.26±0.49	-0.30±0.50	-7.40±0.45
12.25	9410	15.50±0.28	28.77±0.28	3.71±0.28	2.82±0.43	-0.21±0.43	-7.83±0.39
12.00	12527	15.33±0.25	28.96±0.25	4.41±0.25	2.13±0.38	-0.86±0.38	-8.42±0.34
11.75	16842	15.06±0.22	28.72±0.22	4.75±0.22	1.39±0.32	-1.33±0.33	-8.30±0.29
11.50	22936	14.85±0.19	28.57±0.19	5.15±0.19	0.69±0.28	-1.88±0.28	-9.41±0.26
11.25	30955	14.49±0.17	28.65±0.17	5.48±0.17	0.54±0.25	-2.15±0.25	-9.73±0.22
11.00	42149	14.29±0.14	28.50±0.14	5.73±0.14	0.51±0.21	-2.03±0.22	-9.56±0.19
10.75	56686	13.98±0.13	28.11±0.13	5.92±0.13	0.65±0.19	-1.96±0.20	-9.49±0.17
10.50	74710	13.54±0.11	27.48±0.11	5.99±0.11	0.76±0.17	-1.38±0.17	-9.85±0.15
10.25	96055	12.90±0.10	26.98±0.10	6.22±0.10	0.79±0.15	-0.85±0.16	-10.51±0.13
10.00	119880	12.04±0.08	26.58±0.08	6.56±0.08	0.50±0.14	-0.58±0.14	-11.22±0.12
9.75	145752	11.12±0.07	26.27±0.07	6.83±0.07	0.33±0.13	-0.55±0.13	-11.49±0.11
9.50	172728	9.98±0.07	26.01±0.07	7.06±0.07	0.18±0.12	-0.60±0.13	-11.43±0.10
9.25	199244	9.09±0.06	25.76±0.06	7.26±0.06	-0.00±0.12	-0.76±0.12	-11.22±0.09
9.00	225976	8.51±0.06	25.45±0.06	7.43±0.06	-0.21±0.12	-0.83±0.12	-10.94±0.09
8.75	250562	8.34±0.06	25.00±0.06	7.52±0.06	-0.24±0.11	-0.85±0.11	-11.06±0.08
8.50	273889	8.65±0.06	24.47±0.06	7.63±0.06	-0.14±0.11	-0.90±0.11	-11.47±0.08
8.25	296300	9.43±0.05	23.98±0.05	7.67±0.05	-0.10±0.11	-0.93±0.11	-12.39±0.08
8.00	320733	10.47±0.05	23.59±0.05	7.72±0.05	-0.04±0.11	-0.91±0.11	-13.50±0.08
7.75	347258	11.62±0.05	23.46±0.05	7.79±0.05	0.06±0.11	-0.72±0.11	-14.66±0.08
7.50	375367	12.73±0.05	23.58±0.05	7.88±0.05	0.07±0.11	-0.57±0.11	-15.56±0.08
7.25	401070	13.70±0.05	23.88±0.05	7.97±0.05	0.13±0.10	-0.61±0.10	-16.11±0.07
7.00	417071	14.45±0.05	24.57±0.05	8.09±0.05	0.37±0.10	-0.28±0.10	-16.83±0.08
6.75	418459	14.95±0.05	25.48±0.05	8.20±0.05	0.61±0.10	-0.28±0.10	-17.46±0.08
6.50	405412	15.20±0.05	26.58±0.05	8.34±0.05	0.72±0.11	-0.10±0.11	-18.18±0.08
6.25	376332	15.21±0.06	27.93±0.06	8.48±0.06	0.75±0.11	0.02±0.11	-18.99±0.09
6.00	332420	15.10±0.07	29.60±0.07	8.68±0.07	0.69±0.12	0.10±0.12	-20.20±0.10
5.75	276790	14.77±0.08	31.62±0.08	8.85±0.08	0.88±0.13	0.24±0.14	-21.42±0.11
5.50	218552	14.45±0.10	34.09±0.10	8.92±0.10	0.95±0.15	0.25±0.16	-22.72±0.13
5.25	166997	14.06±0.11	36.85±0.11	9.04±0.11	0.39±0.18	0.22±0.18	-24.05±0.16
5.00	126335	13.75±0.14	40.31±0.14	9.08±0.14	0.29±0.21	-0.17±0.21	-25.49±0.19
4.75	94575	13.59±0.17	44.52±0.17	9.14±0.17	0.13±0.25	0.36±0.25	-27.51±0.23
4.50	70530	13.68±0.20	49.18±0.20	9.37±0.20	-0.20±0.30	0.67±0.30	-29.60±0.28
4.25	53084	13.93±0.25	54.24±0.25	9.50±0.25	0.05±0.35	0.98±0.36	-31.28±0.35
4.00	40550	14.63±0.29	60.15±0.29	9.45±0.29	0.46±0.42	0.70±0.43	-33.29±0.42
3.75	31430	15.48±0.35	66.16±0.35	9.42±0.35	-0.07±0.49	-0.05±0.51	-34.84±0.51
3.50	24730	16.20±0.41	72.37±0.41	9.80±0.41	-0.91±0.58	-0.29±0.60	-36.12±0.61
3.25	19871	17.51±0.48	78.65±0.48	9.61±0.48	-1.11±0.68	-0.96±0.70	-37.04±0.73
3.00	16167	18.35±0.56	85.82±0.56	9.16±0.56	-1.07±0.80	-1.06±0.81	-39.66±0.86
2.75	13375	19.74±0.66	93.26±0.66	8.84±0.66	-1.17±0.93	-1.05±0.94	-40.33±1.02
2.50	11135	20.30±0.76	100.65±0.76	9.12±0.76	-2.37±1.07	0.10±1.08	-41.04±1.19
2.25	9481	21.55±0.87	108.27±0.87	10.47±0.87	-2.93±1.22	1.16±1.23	-42.33±1.36
2.00	8118	21.78±0.99	116.56±0.99	10.80±0.99	-4.87±1.39	0.23±1.40	-43.44±1.55
1.75	7121	22.64±1.11	123.98±1.11	9.62±1.11	-6.11±1.54	-2.77±1.55	-44.74±1.74
1.50	6084	22.53±1.26	132.80±1.26	9.33±1.26	-6.41±1.73	-3.58±1.75	-44.18±1.97
1.25	5172	22.59±1.46	141.34±1.46	9.56±1.46	-7.76±1.99	-3.27±1.99	-45.37±2.26
1.00	4463	22.68±1.66	147.17±1.66	7.37±1.66	-10.12±2.24	-3.08±2.21	-44.29±2.51
0.75	3869	22.22±1.89	154.05±1.89	7.85±1.89	-10.87±2.50	-0.64±2.46	-46.63±2.80
0.50	3399	22.08±2.09	161.86±2.09	10.04±2.09	-8.25±2.75	5.02±2.69	-46.09±3.07
0.25	2978	22.99±2.31	171.72±2.31	13.92±2.31	-6.41±3.02	4.24±3.01	-50.13±3.41
0.00	2663	21.57±2.52	180.78±2.52	13.87±2.52	-7.30±3.30	-0.52±3.25	-53.29±3.71

Table A2. The O–M model parameters for stellar systems with $r' = 1.0$ kpc. R is the Galactocentric distance to centroids, in kpc; N_{stars} is the number of stars containing in each stellar system; the O–M model parameters are in $\text{km s}^{-1} \text{kpc}^{-1}$.

R	N_{stars}	M_{23}^+	M_{13}^+	M_{12}^+	M_{11}^+	M_{22}^+	M_{33}^+
16.00	202	-6.92±3.24	-5.18±3.19	10.08±3.00	-10.29±4.18	-3.88±4.32	-0.28±4.82
15.75	242	-7.93±2.79	1.40±2.77	8.17±2.63	-4.49±3.67	-3.11±3.76	-1.38±4.13
15.50	296	-5.45±2.50	2.03±2.47	7.80±2.32	-1.95±3.25	-4.07±3.32	-2.92±3.74
15.25	372	-2.99±2.09	1.28±2.04	10.69±1.96	-0.90±2.71	-2.61±2.83	-7.29±3.06
15.00	469	-3.37±2.01	-0.89±2.01	9.37±1.91	-2.16±2.70	1.64±2.70	-8.96±2.97
14.75	619	-3.54±1.78	-0.67±1.82	9.94±1.72	-4.18±2.50	-0.23±2.37	-6.18±2.64
14.50	809	-4.93±1.58	-0.33±1.59	9.38±1.49	-4.28±2.14	-1.40±2.08	-4.31±2.37
14.25	1055	-4.33±1.33	0.02±1.34	9.66±1.29	-2.85±1.84	0.17±1.80	-2.48±1.95
14.00	1383	-3.97±1.13	0.15±1.13	10.28±1.07	-0.09±1.51	0.52±1.53	-3.71±1.67
13.75	1815	-5.96±1.04	0.11±1.04	9.99±0.98	0.10±1.37	-0.07±1.39	-4.23±1.56
13.50	2396	-5.97±0.94	-0.68±0.94	8.72±0.88	1.47±1.25	-1.60±1.25	-3.65±1.40
13.25	3160	-5.69±0.80	-0.70±0.80	9.92±0.75	1.43±1.06	-1.16±1.06	-3.70±1.20
13.00	4183	-5.07±0.69	-1.02±0.69	9.79±0.64	1.63±0.91	-0.99±0.91	-4.58±1.03
12.75	5438	-4.96±0.59	-2.15±0.59	9.64±0.55	1.07±0.78	-0.01±0.77	-3.79±0.90
12.50	7209	-4.10±0.49	-2.35±0.50	9.20±0.45	0.72±0.65	0.16±0.64	-3.89±0.75
12.25	9410	-2.94±0.43	-2.36±0.43	8.77±0.39	0.44±0.56	0.56±0.55	-3.38±0.65
12.00	12527	-2.77±0.38	-2.76±0.38	8.82±0.34	1.23±0.49	0.87±0.48	-2.69±0.58
11.75	16842	-1.93±0.32	-3.05±0.33	9.20±0.29	1.41±0.42	0.80±0.41	-2.03±0.50
11.50	22936	-1.63±0.28	-2.86±0.28	9.60±0.26	1.19±0.37	0.94±0.35	-1.28±0.43
11.25	30955	-1.37±0.25	-2.63±0.25	10.48±0.22	1.25±0.33	0.85±0.31	-0.65±0.39
11.00	42149	-1.08±0.21	-2.66±0.22	11.71±0.19	1.03±0.28	0.59±0.26	-0.14±0.34
10.75	56686	-0.86±0.19	-2.49±0.20	12.56±0.17	1.48±0.25	0.42±0.23	0.22±0.30
10.50	74710	-0.70±0.17	-2.36±0.17	12.66±0.15	2.46±0.22	0.45±0.20	0.26±0.27
10.25	96055	-0.65±0.15	-2.11±0.16	12.53±0.13	3.34±0.19	0.18±0.18	-0.02±0.25
10.00	119880	-0.40±0.14	-2.00±0.14	12.44±0.12	4.30±0.17	-0.09±0.16	-0.10±0.23
9.75	145752	-0.27±0.13	-1.60±0.13	12.44±0.11	4.94±0.16	-0.60±0.15	-0.48±0.22
9.50	172728	-0.10±0.12	-1.42±0.13	12.41±0.10	4.70±0.14	-0.81±0.14	-0.59±0.21
9.25	199244	0.08±0.12	-1.41±0.12	12.76±0.09	3.54±0.13	-1.06±0.13	-0.78±0.20
9.00	225976	0.24±0.12	-1.23±0.12	13.15±0.09	1.68±0.13	-1.26±0.12	-0.85±0.20
8.75	250562	0.33±0.11	-1.06±0.11	13.82±0.08	-0.59±0.12	-1.11±0.12	-0.84±0.19
8.50	273889	0.25±0.11	-1.08±0.11	14.45±0.08	-2.81±0.12	-0.82±0.11	-0.68±0.19
8.25	296300	0.31±0.11	-1.07±0.11	14.90±0.08	-4.54±0.11	-0.37±0.11	-0.60±0.19
8.00	320733	0.20±0.11	-0.99±0.11	14.92±0.08	-5.22±0.11	-0.23±0.11	-0.38±0.19
7.75	347258	-0.04±0.11	-0.95±0.11	14.73±0.08	-5.33±0.11	-0.11±0.11	-0.39±0.19
7.50	375367	-0.19±0.11	-0.88±0.11	14.52±0.08	-4.50±0.11	-0.12±0.11	-0.13±0.18
7.25	401070	-0.26±0.10	-1.00±0.10	14.50±0.07	-3.29±0.11	-0.14±0.11	0.21±0.18
7.00	417071	-0.47±0.10	-0.79±0.10	14.20±0.08	-2.11±0.11	0.07±0.11	0.27±0.18
6.75	418459	-0.64±0.10	-0.84±0.10	13.95±0.08	-1.21±0.11	0.36±0.11	0.40±0.18
6.50	405412	-0.69±0.11	-0.84±0.11	13.64±0.08	-0.46±0.12	0.79±0.11	0.37±0.18
6.25	376332	-0.67±0.11	-0.69±0.11	13.02±0.09	0.12±0.13	1.52±0.12	0.53±0.19
6.00	332420	-0.55±0.12	-0.71±0.12	12.55±0.10	0.61±0.14	2.35±0.13	0.70±0.20
5.75	276790	-0.67±0.13	-0.67±0.14	12.11±0.11	1.02±0.16	3.28±0.15	0.98±0.22
5.50	218552	-0.81±0.15	-0.42±0.16	11.79±0.13	0.98±0.19	3.84±0.18	1.11±0.25
5.25	166997	-0.53±0.18	-0.22±0.18	11.69±0.16	1.44±0.22	4.19±0.22	1.55±0.28
5.00	126335	-0.58±0.21	-0.12±0.21	11.06±0.19	1.06±0.27	4.70±0.27	1.55±0.33
4.75	94575	-0.80±0.25	0.08±0.25	10.57±0.23	0.27±0.33	4.26±0.33	1.67±0.38
4.50	70530	-0.82±0.30	0.46±0.30	9.86±0.28	-0.13±0.40	3.30±0.40	1.40±0.44
4.25	53084	-0.76±0.35	0.44±0.36	9.34±0.35	-0.62±0.50	2.34±0.49	0.65±0.51
4.00	40550	-1.07±0.42	0.22±0.43	9.35±0.42	-2.50±0.61	0.57±0.59	0.06±0.60
3.75	31430	-0.75±0.49	0.26±0.51	8.79±0.51	-3.71±0.74	-0.50±0.70	-1.20±0.69
3.50	24730	0.24±0.58	0.02±0.60	10.10±0.61	-4.69±0.89	-1.53±0.85	-1.67±0.80
3.25	19871	0.32±0.68	-0.85±0.70	10.14±0.73	-4.62±1.05	-1.52±1.01	-0.37±0.91
3.00	16167	2.00±0.80	-1.52±0.81	8.70±0.86	-3.03±1.24	-2.84±1.20	0.65±1.05
2.75	13375	3.67±0.93	-0.42±0.94	9.19±1.02	-3.70±1.45	-4.84±1.42	0.50±1.19
2.50	11135	4.57±1.07	-0.08±1.08	7.76±1.19	-3.57±1.69	-5.06±1.66	0.85±1.35
2.25	9481	5.87±1.22	-1.78±1.23	7.85±1.36	-3.04±1.93	-6.05±1.91	1.34±1.52
2.00	8118	6.80±1.39	-2.56±1.40	8.61±1.55	-2.18±2.21	-5.08±2.18	1.82±1.71
1.75	7121	7.40±1.54	-0.91±1.55	10.17±1.74	-2.72±2.48	-7.38±2.45	2.96±1.87
1.50	6084	6.47±1.73	-0.13±1.75	7.19±1.97	3.56±2.80	-6.93±2.77	1.86±2.09
1.25	5172	7.30±1.99	0.35±1.99	7.31±2.26	-2.66±3.20	-4.45±3.20	3.91±2.37
1.00	4463	6.80±2.24	2.52±2.21	11.92±2.51	4.67±3.52	-9.54±3.59	5.17±2.67
0.75	3869	5.53±2.50	-0.96±2.46	12.49±2.80	3.77±3.92	-9.24±4.01	8.42±2.98
0.50	3399	5.19±2.75	-6.60±2.69	12.22±3.07	0.38±4.26	-8.55±4.43	7.43±3.28
0.25	2978	10.07±3.02	-6.11±3.01	10.28±3.41	-1.12±4.82	-2.53±4.83	6.17±3.62
0.00	2663	10.66±3.30	-2.32±3.25	9.39±3.71	-4.27±5.18	-2.13±5.31	5.78±3.92